10970 *Inorg. Chem.* **2010**, *49*, 10970–10976
DOI: 10.1021/ic1011082

Inorganic Chemistry
Article

Site-Selective Lanthanide Doping in a Nonanuclear Yttrium(III) Cluster Revealed by Crystal Structures and Luminescence Spectra

François Baril-Robert,[†] Sarah Petit,[‡,§] Guillaume Pilet,[‡] Guillaume Chastanet,[‡,⊥] Christian Reber,*[,†] and Dominique Luneau*[,‡]

[†]*Département de Chimie, Université de Montréal, Montréal, Québec H3C 3J7, Canada, and* [‡]*Laboratoire des Multimatériaux et Interfaces (UMR 5615), Université Claude Bernard Lyon 1, Campus de la Doua, 69622 Villeurbanne Cedex, France.* [§]*Present address: Institut Néel, CNRS, 25 avenue des Martyrs, BP 166, 38042 Grenoble Cedex 09, France.* [⊥]*Present address: CNRS, Université de Bordeaux, ICMCB, 87 avenue du Dr. A. Schweitzer, F-33608 Pessac, France.*

Received July 14, 2010

A series of lanthanide-doped nonanuclear yttrium(III) clusters with general formulas $(Y_{9-x}Ln_x)(acac)_{16}(\mu^3\text{-}OH)_8(\mu^4\text{-}O)(\mu^4\text{-}OH)$ (Ln = Pr, Eu, Tb, Dy, and Yb) were synthesized. Characterization by single-crystal X-ray diffraction allowed for analysis of relative populations of yttrium ($Z = 39$) and dopant trivalent lanthanide ($Z = 59-70$) at every crystallographic metal position. Nonuniform distribution of ions along the three different sites seems to be correlated to the site volume and the ratio of ionic radii. In support, luminescence spectra of europium(III)-doped nonanuclear clusters were measured over a wide range of dopant concentrations. Emission intensities of peaks characteristic of specific sites correlate well with the site population determined through X-ray diffraction.

Introduction

Although a general approach to the fabrication of nanoentities in a precisely controlled manner is not yet available, it is widely accepted that coordination chemistry offers an attractive approach to create sophisticated and single-sized nanoscale polynuclear clusters relevant to chemistry, physics, and biology. In this context and as part of our focus on the magnetism and optical properties of polynuclear metal complexes incorporating lanthanide ions,[1−3] we recently reinvestigated the coordination chemistry of β-diketone ligands. We reported an interesting case of rational cluster nuclearity control that allowed the study of the optical properties of penta-, octa-, and nonanuclear europium(III) and terbium(III) clusters.[4]

Our interest in lanthanide clusters comes from the well-established relevance of lanthanide ions and their partially filled 4f shell for both magnetism and optical properties.[5−7] Among them, some exhibit strong magnetic anisotropy due to large spin−orbit coupling, and in the past few years, several complexes based on lanthanide ions[8−10] or combined with 3d transition-metal ions[2,10−13] were reported to exhibit single-molecule-magnet behavior.[2,9−11,13,14]

Additionally, lanthanide compounds have attracted extensive attention because of their wide range of emission wavelengths, and they have excellent luminescence properties[15] and therefore have received much attention for luminescence applications.[6,7] Spectroscopic properties are

*To whom correspondence should be addressed. E-mail: christian.reber@umontreal.ca (C.R.), luneau@univ-lyon1.fr (D.L.).

(1) Aronica, C.; Chastanet, G.; Pilet, G.; Le Guennic, B.; Robert, V.; Wernsdorfer, W.; Luneau, D. *Inorg. Chem.* **2007**, *46*, 6108–6119.
(2) Aronica, C.; Pilet, G.; Chastanet, G.; Wernsdorfer, W.; Jacquot, J.-F.; Luneau, D. *Angew. Chem., Int. Ed.* **2006**, *45*, 4659–4662.
(3) Bussière, G.; Beaulac, R.; Bélisle, H.; Lescop, C.; Luneau, D.; Rey, P.; Reber, C. *Top. Curr. Chem.* **2004**, *241*, 97–118.
(4) Petit, S.; Baril-Robert, F.; Pilet, G.; Reber, C.; Luneau, D. *Dalton Trans.* **2009**, 6809–6815.
(5) Benelli, C.; Gatteschi, D. *Chem. Rev.* **2002**, *102*, 2369–2387.
(6) Bünzli, J.-C. G. *Acc. Chem. Res.* **2006**, *39*, 53–61.
(7) Bünzli, J.-C. G.; Piguet, C. *Chem. Rev.* **2002**, *102*, 1897–1928.
(8) Gamer, M. T.; Lan, Y.; Roesky, P. W.; Powell, A. K.; Clérac, R. *Inorg. Chem.* **2008**, *47*, 6581–6583.
(9) Ishikawa, N.; Sugita, M.; Wernsdorfer, W. *J. Am. Chem. Soc.* **2005**, *127*, 3650–36510.
(10) Tang, J.; Hewitt, I.; Madhu, N. T.; Chastanet, G.; Wernsdorfer, W.; Anson, C. E.; Benelli, C.; Sessoli, R.; Powell, A. K. *Angew. Chem., Int. Ed.* **2006**, *45*, 1729–1733.
(11) Mori, F.; Nyui, T.; Ishida, T.; Nogami, T.; Choi, K.-Y.; Nojiri, H. *J. Am. Chem. Soc.* **2006**, *128*, 1440–1441.
(12) Zaleski, C. M.; Depperman, E. C.; Kampf, J. W.; Kirk, M. L.; Pecoraro, V. L. *Angew. Chem., Int. Ed* **2004**, *43*, 3912–3914.
(13) Osa, S.; Kido, T.; Matsumoto, N.; Re, N.; Pochaba, A.; Mrozinski, J. *J. Am. Chem. Soc.* **2004**, *126*, 420–421.
(14) Roesky, P. W.; Canseco-Melchor, G.; Zulys, A. *Chem. Commun.* **2004**, 738–739.
(15) (a) Ehlert, O.; Thomann, R.; Darbandi, M.; Nann, T. *ACS Nano* **2008**, *2*, 120–124. (b) Wang, F.; Liu, X. G. *J. Am. Chem. Soc.* **2008**, *130*, 5642–5643. (c) Su, Y. G.; Li, L. P.; Li, G. S. *Chem. Commun.* **2008**, 4004–4006. (d) Lin, C. K.; Zhang, C. M.; Lin, J. *J. Phys. Chem. C* **2007**, *111*, 3300–3307. (e) Lin, C. K.; Luo, Y.; You, H.; Quan, Z. W.; Zhang, J.; Fang, J.; Lin, J. *Chem. Mater.* **2006**, *18*, 458–464. (f) Lin, C. K.; Wang, H.; Kong, D. Y.; Yu, M.; Liu, X. M.; Wang, Z. L.; Lin, J. *Eur. J. Inorg. Chem.* **2006**, 3667–3675.

Published on Web 10/25/2010

Table 1. Results of the Structural Refinement for $[Y_{9-x}Ln_x]$ with Ln = Yb, Dy, Tb, and Pr

	$[Y_{7.34}Yb_{1.66}]$ (**1**), 18.4% of Yb^{III}	$[Y_{7.02}Dy_{1.98}]$ (**2**), 22.0% of Dy^{III}	$[Y_{7.05}Tb_{1.95}]$ (**3**), 21.7% of Tb^{III}	$[Y_{8.77}Pr_{0.23}]$ (**4**), 2.6% of Pr^{III}
refined formula	$C_{80}H_{121}O_{42}Y_{7.34}Yb_{1.66}$	$C_{80}H_{122}O_{42.5}Y_{7.02}Dy_{1.98}$	$C_{80}H_{121}O_{42}Y_{7.05}Tb_{1.95}$	$C_{80}H_{122}O_{45}Y_{8.77}Pr_{0.23}$
fw ($g \cdot mol^{-1}$)	2694.6	2709.7	2691.5	2615.9
cryst syst	tetragonal			
space group	*P*4/*n* (No. 85)			
a (Å)	19.1633(3)	19.251(3)	19.1463(2)	19.0060(4)
c (Å)	15.4901(4)	15.5601(4)	15.5273(2)	15.5001(3)
V ($Å^3$)	5688.5(2)	5765(2)	5692.0(1)	5599.1(2)
Z	2			
T (K)	290			
λ(Mo Kα), Å	0.710 73			
D ($g \cdot cm^{-3}$)	1.573	1.561	1.570	1.552
μ (mm^{-1})	5.120	4.829	4.818	4.665
no. of indep reflns	6771	7073	6777	6673
R_{int}	0.046	0.040	0.032	0.072
$R(F)$ $[I > 3\sigma(F_0)]^a$	0.0696	0.0359	0.0356	0.0463
$R_w(F)$ $[I > 3\sigma(F_0)]^b$	0.0721	0.0414	0.0404	0.0509
S	1.01	1.01	1.11	1.07
no. of reflns	3695	4051	3936	3071
no. of refined param	259	310	308	309
$\Delta\rho_{max}$ ($e \cdot Å^{-3}$)	2.62	1.81	2.35	2.08
$\Delta\rho_{min}$ ($e \cdot Å^{-3}$)	−2.31	−1.71	−1.80	−1.09

$^a R(F) = \sum(|F_o| - |F_c|)/\sum|F_o|$. $^b R_w(F) = \sum[w(F_o^2 - F_c^2)/\sum wF_o^4]^{1/2}$.

also of interest in the study of magnetic systems because their narrow emission and absorption bands, environment dependency, and multiple emissive transitions give access to the precise energies of the spin−orbit components and splitting caused by crystal-field perturbations.[3,16]

In a previous report, we showed how substituted β-diketone ligands allowed size control of a series of lanthanide clusters whose nuclearity (5, 8, or 9) increased with a decrease in the steric hindrance of the substituent.[4] Using acetyl acetone, we thus synthesized nonanuclear complexes containing Y^{III}, Eu^{III}, and Tb^{III} ions. Luminescence spectroscopy of the europium and terbium compounds showed the relationship between the luminescence properties and lanthanide local geometry, and for $[Eu_9]$, we were able to assign some emission peaks to specific inner-cluster sites. We now report the doping of $[Y_9]$ clusters with several trivalent lanthanide ions (Ln = Pr, Eu, Tb, Dy, and Yb) and their effect on the structural and spectroscopic properties. In this study, we are interested in the effect of the lanthanide characteristics, such as ionic radii, on the site selectivity of the doping.

We first synthesized a series of mixed $[Y_{9-x}Ln_x]$ nonanuclear clusters (Ln = Pr, Eu, Tb, Dy, and Yb) with a low concentration of the lanthanide dopant. We were able to determine the nonuniform Y:Ln distribution on each metallic crystallographic position for all clusters and to observe the importance of the relative ionic radius on the doping uniformity. On the basis of this result, we investigated the luminescence spectra at all dopant concentrations in the $[Y_{9-x}Eu_x]$ nonanuclear cluster. To the best of our knowledge, this is the first study of doped nanoclusters showing a clear relationship between lanthanide luminescence and nonuniform doping.

Experimental Section

Single-Crystal X-ray Diffraction (XRD). Diffraction data sets were collected on a Nonius Kappa CCD and using the appropriate software.[17] All of the structures were solved by direct methods using the *SIR97* program,[18] combined with Fourier difference syntheses, and refined against *F* using reflections with $I/\sigma(I) > 3$ and using the *CRYSTALS* program.[19] In each structure, all atomic displacements for non-H atoms have been refined anisotropically. H positions in the C−H bonds have been calculated and H positions in the O−H bonds refined by Fourier difference, keeping some restraints (riding mode).

For all cases, Y atoms were first positioned on all of the crystallographically independent metallic sites (Ln1, Ln2, and Ln3). After several cycles of refinement, the electronic density on some metallic positions, depending on the ion and doping level, was not fully described by a single Y^{III} ion. Lanthanide atoms Dy (**1**), Yb (**2**), Tb (**3**), Pr (**4**), and Eu (**5**−**8**) were then introduced with the same position and atomic displacement parameters as those of the Y atom. For each crystallographic site, the sum of the occupancies was restrained to represent a fully occupied position. The Y/Ln statistical occupation was then refined, keeping restraints on the metallic positions and displacements.

X-ray crystallographic data and refinement details for compounds with Dy, Yb, Tb, and Pr ions are summarized in Table 1. In the case of compounds with Eu ions, the information is given in Table 2.

Spectroscopy. Raman and luminescence spectra were measured with a Renishaw 3000 Raman imaging microscope at 488, 514, and 785 nm excitation laser wavelengths. The microscope was used to focus the light onto a spot of approximately 1 μm in diameter and to collect the scattered light. The backscattered Raman light was detected with a Peltier cooled CCD detector. This instrument was also used to measure luminescence spectra (λ_{ex} = 488 nm). Sample temperatures were controlled with a Linksys 500 cryostat using cold nitrogen gas.

Results and Discussion

Synthesis. All chemicals, ligands, and solvents were used as received; all preparations and manipulations were performed under aerobic conditions.

(16) Vicentini, G.; Zinner, L. B.; Zukerman-Schpector, J.; Zinner, K. *Coord. Chem. Rev.* **2000**, *196*, 353–382.
(17) *Nonius*; Nonius BV: Delft, The Netherlands, 1999.
(18) Cascarano, G.; Altomare, A.; Giacovazzo, C.; Guagliardi, A.; Moliterni, A. G. G.; Siliqi, D.; Burla, M. C.; Polidori, G.; Camalli, M. *Acta Crystallogr.* **1996**, *A52*, C–79.
(19) Watkin, D. J.; Prout, C. K.; Carruthers, J. R.; Betteridge, P. W. *CRYSTALS*; Chemical Crystallography Laboratory: Oxford, U.K., 1999; issue 11.

Table 2. Results of the Structural Refinement for $[Y_{9-x}Eu_x]$ with $x = 0.40$, 0.98, 2.92, and 4.35

	$[Y_{8.60}Eu_{0.40}]$ (**5**), 4.4% of Eu^{III}	$[Y_{8.02}Eu_{0.98}]$ (**6**), 10.9% of Eu^{III}	$[Y_{6.08}Eu_{2.92}]$ (**7**), 32.4% of Eu^{III}	$[Y_{4.65}Eu_{4.35}]$ (**8**), 48.3% of Eu^{III}
refined formula	$C_{80}H_{123}O_{43}Y_{8.60}Eu_{0.40}$	$C_{80}H_{122}O_{42.5}Y_{8.02}Eu_{0.98}$	$C_{80}H_{122}O_{42.5}Y_{6.08}Eu_{2.92}$	$C_{80}H_{122.5}O_{43.5}Y_{4.65}Eu_{4.35}$
fw ($g \cdot mol^{-1}$)	2598.4	2625.75	2747.8	2853.9
cryst syst	tetragonal			
space group	*P*4/*n* (No. 85)			
a (Å)	19.2950(9)	19.1041(3)	19.2610(6)	19.2299(6)
c (Å)	15.5604(6)	15.5149(4)	15.5773(6)	15.4407(6)
V ($Å^3$)	5793.1(4)	5662.4(2)	5779.0(3)	5709.8(3)
Z	2			
T (K)	290			
λ(Mo Kα), Å	0.710 73			
D ($g \cdot cm^{-3}$)	1.490	1.540	1.579	1.662
μ (mm^{-1})	4.541	4.668	4.647	4.760
no. of indep reflns	6787	5579	6886	6867
R_{int}	0.128	0.036	0.184	0.093
$R(F)$ $[I > 3\sigma(F_0)]^a$	0.0508	0.1233	0.0668	0.0414
$R_w(F)$ $[I > 3\sigma(F_0)]^b$	0.0462	0.1204	0.0750	0.0584
S	1.15	1.08	1.13	1.20
no. of reflns	2506	3535	3089	3168
no. of refined param	288	288	299	325
$\Delta\rho_{max}$ ($e \cdot Å^{-3}$)	1.04	3.09	3.18	0.66
$\Delta\rho_{min}$ ($e \cdot Å^{-3}$)	−0.54	−3.32	−3.82	−0.75

$^a R(F) = \sum(|F_o| - |F_c|)/\sum|F_o|$. $^b R_w(F) = \sum[w(F_o^2 - F_c^2)/\sum wF_o^4]^{1/2}$.

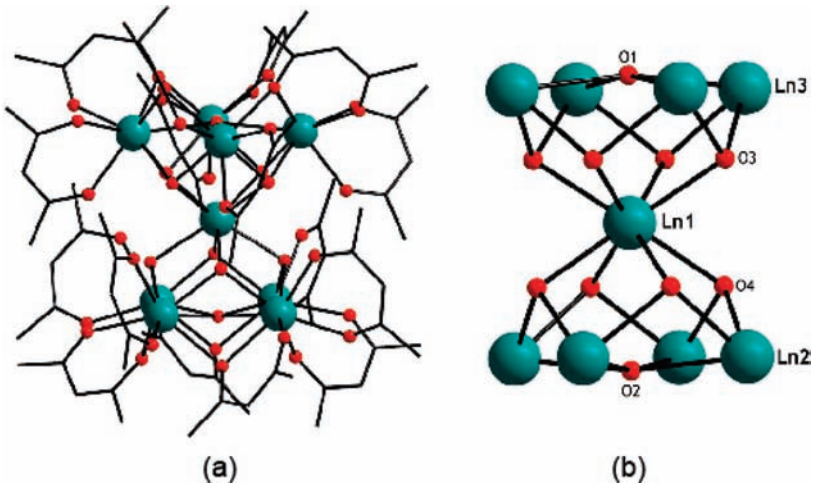

Figure 1. (a) General representation of a $[Ln_9]$ cluster (H atoms have been omitted for clarity) and (b) a simplified view showing labels of important atomic positions.

$[Y_{9-x}Ln_x(acac)_{16}(\mu_3\text{-OH})_8(\mu_4\text{-O})(\mu_4\text{-OH})] \cdot yH_2O$ (Ln = Pr, Eu, Tb, Dy, and Yb). Syntheses of pure $[Ln_9]$ nonanuclear compounds were previously reported (Ln = Y, Dy, and Tb).[4] A similar method was used to obtain $[Y_{9-x}Ln_x(acac)_{16}(\mu_3\text{-OH})_8(\mu_4\text{-O})(\mu_4\text{-OH})] \cdot yH_2O$-doped (named $[Y_{9-x}Ln_x]$) compounds. As an example, a mixture of yttrium chloride (0.88 mmol) and $LnCl_3 \cdot 6H_2O$ (0.11 mmol; Ln = Pr, Eu, Tb, Dy, and Yb) was dissolved in 5 mL of methanol. Then acetyl acetone (0.2 mL, 2 mmol) and triethylamine (0.4 mL, 3 mmol) were added to the clear solution. The resulting solution was transferred to a sealed bottle and was left to cool in a freezer. After 3 days, colorless or, depending on the lanthanide, slightly colored cubic crystals suitable for XRD were collected. Other Ln:Y doping ratios were obtained by varying the chloride salt proportions.

Crystal Structure Description. We recently reported the structures of neutral $[Y_9]$, $[Tb_9]$, and $[Eu_9]$ nonanuclear clusters, which can be described as two pentanuclear square pyramids sharing the same top Ln^{III} ion (Figure 1).[4] All triangular faces of these pyramids are capped by μ_3-OH groups, while the four Ln atoms of the two square planes are connected by disordered μ_4-(O,OH) groups. To keep the overall neutrality of the clusters, the occupancy of the H atoms supported by the μ_4-(O,OH) disordered groups was assumed to be 50%.[4] The torsion angle between the pyramid moieties is approximately 45°. Thus, the central Ln^{III} atom (Ln1) surrounded by eight μ_3-OH groups is in a near-perfect square-antiprism configuration (D_{4d}), while peripheral Ln ions in the base plane of the pyramids have a highly distorted, low-symmetry coordination geometry.

In this work, we were able to determine by single-crystal XRD the structures of eight mixed nonanuclear clusters $[Y_{9-x}Ln_x]$ (Ln = Pr, Eu, Tb, Dy, and Yb) with different concentrations of Ln^{III} ions. As expected, all compounds crystallize in the same space group, *P*4/*n* (No. 85), confirmed by the observed systematic extinctions. Therefore, all compounds are isostructural, and all form $[Y_{9-x}Ln_x(acac)_{16}(\mu_3\text{-OH})_8(\mu_4\text{-O})(\mu_4\text{-OH})] \cdot yH_2O$ clusters with little variation in the number of solvated

Table 3. Amount of Ln Ion in Reaction Mixtures, on the Central Position (Ln1), on the Peripheral Positions (Ln2 and Ln3), and per Clusters[a]

				local concentration (%)[b]			overall concentration (%)[c]		total, n_t (%)[d]	analysis[e]
cluster	Ln	R (Å)	reaction mixture (%)[f] (n_r)	Ln1	Ln2	Ln3	Ln1 (n_c)	Ln2 + Ln3 (n_p)	XRD	EDX
$[Y_{7.34}Yb_{1.66}]$	Yb	0.985	25	6.6	21.2	18.6	0.7	17.7	18.4	17.6
$[Y_9]^4$	Y	1.019	0	0	0	0	0	0	0	
$[Y_{7.02}Dy_{1.98}]$	Dy	1.027	25	47.6	18.4	19.2	5.3	16.7	22.0	18.9
$[Y_{7.05}Tb_{1.95}]$	Tb	1.040	25	46.8	18.0	19.0	5.2	16.5	21.7	21.0
$[Y_{8.60}Eu_{0.40}]$	Eu	1.066	5	21.6	2.6	2.1	2.4	2.0	4.4	[g]
$[Y_{8.02}Eu_{0.98}]$			15	36.8	8.5	6.9	4.1	6.8	10.9	8.9
$[Y_{6.08}Eu_{2.92}]$			35	86.4	22.3	29.0	9.6	22.8	32.4	29.9
$[Y_{4.65}Eu_{4.35}]$			50	100	40.4	43.5	11.1	37.2	48.3	49.1
$[Eu_9]^4$			100	100	100	100	11.1	88.9	100	
$[Y_{8.77}Pr_{0.23}]$	Pr	1.126	25	22.8	0	0	2.5	0	2.5	[g]

[a] In all cases, the amount holds for ratio Ln/(Y + Ln). [b] Determined from single-crystal XRD structure refinement of the site occupation with Ln + Y = 100. [c] The overall concentration considering a site multiplicity of $^1/_9$ for Ln1 and $^4/_9$ for both Ln2 and Ln3. [d] The total concentration in the cluster calculated from on-site XRD structure refinement data as $^1/_9$Ln1 (%) + $^4/_9$Ln2 (%) + $^4/_9$Ln3 (%). [e] Corresponding to the average of data collected on 10 single crystals. [f] The concentration in the reaction mixtures. [g] Due to the low percentage of introduced Ln^{III} element. EDX results were not significant and have not been included in the table.

water molecules. Moreover, these structures are all isostructural to the $[Y_9]$ nonanuclear cluster previously reported.[4] Because of the large difference in the atomic number between Y and the Ln dopant ion, it was possible to determine the dopant percentage on every metallic site (Ln1, Ln2, and Ln3). Nonanuclear clusters presented here only differ by the nature and overall relative concentration of the Ln dopant ion.

As for the yttrium $[Y_9]$ cluster, the $[Y_{9-x}Ln_x]$-doped clusters are neutral. From a crystallographic point of view, the asymmetric unit is composed of three independent Ln atoms. The central atom (Ln1) is on a 2c special Wyckoff position, and a total of eight peripheral lanthanide sites (Ln2 and Ln3) are on two different 8g general Wyckoff positions. Four acetylacetonate ligands, two μ_3-OH groups, (8g Wickoff position), and two disordered μ_4-(O,OH) groups on special 2c Wyckoff positions complete the nonanuclear cluster. Regarding the symmetry elements of the space group used during the refinement, the final formula is $[Y_{9-x}Ln_x(acac)_{16}(\mu_3\text{-OH})_8(\mu_4\text{-O})(\mu_4\text{-OH})]\cdot yH_2O$, where Y positions are doped by Ln^{III} ions (Ln = Pr, Eu, Tb, Dy, and Yb). The local lanthanide population on each of the three crystallographic positions (Ln1, Ln2, and Ln3) has been determined from the site occupation factor refinement considering a mixture of yttrium and lanthanide. Further, for all clusters, the total amount of lanthanide (Ln/Y + Ln) per cluster calculated (%) from these local populations [$^1/_9$Ln1 (%) + $^4/_9$Ln2 (%) + $^4/_9$Ln3 (%)] has been found to be in agreement with energy-dispersive X-ray (EDX) (transmission electron microscopy) analysis (Table S1 in the Supporting Information).

Our original goal was to design mixed-lanthanide clusters with site-selective doping. Chemical selectivity should be induced by the relative cavity sizes versus the Y:Ln ionic radii ratio. In order to explore this approach, we first synthesized compounds based on $[Y_9]$ clusters doped with different lanthanides (Ln = Pr, Eu, Tb, Dy, and Yb) having significantly different ionic radii. First, using in the reaction a mixture of yttrium and lanthanide salts containing a constant amount of lanthanides (Ln/Y + Ln = 25%), we studied how the ionic radius of the lanthanide dopant ion influences the selectivity.

In all cases, a nonuniform distribution of the dopant ion is observed (Table 3). At first glance, a dopant ion such as Yb^{III} with a smaller ionic radius than Y^{III} appears to prefer peripheral sites (Ln2 and Ln3) compared to the central site (Ln1). In contrast, dopant ions with larger radii (Dy, Tb, Eu, and Pr) favor the central site. This is in agreement with our previous report that, in $[Ln_9]$ clusters, the central position is significantly larger than the peripheral position.[4] As an example, in the $[Y_9]$ cluster, the average Y−O bond length for the central site is slightly longer than that for the peripheral sites (2.417 Å vs 2.362 and 2.369 Å). Moreover, all Y−O bond lengths for the central site (Y1) are very similar (from 2.410 to 2.424 Å), but for peripheral sites, they vary from 2.267 to 2.541 Å and from 2.293 to 2.567 Å for Y2 and Y3, respectively. In view of these bond-length variations for peripheral sites, the average bond lengths may not be the most realistic to evaluate the different site sizes available to the dopant Ln ions on each crystallographically independent site. Better, considering only the shortest Y−O bond lengths (2.41 Å for Y1 and 2.267 and 2.293 Å for Y2 and Y3, respectively), we found that the volume of the central site (58.6 $Å^3$) is almost 20% bigger than that the peripheral sites (48.8 and 50.5 $Å^3$ for Y2 and Y3, respectively). This rationalizes the tendency of incorporated Ln^{III} ions to prefer the central site.

To support our assumption about the coordination cavity-size-driven selectivity, we also compared the local dopant amount (n_c) in the central position (Ln1) to the total dopant amount (n_t) on the overall cluster (Table 3). Figure 2 shows a plot that gives a good overview of the doping selectivity for the selected Ln ions. In Figure 2, a line with a slope of 1 represents a situation with all dopant ions occupying central positions, while a slope of 0 would be a perfect selectivity toward peripheral sites. A slope of $^1/_9$ would correspond to a purely statistical distribution with no apparent selectivity. The comparison is, of course, valid when the total amount is small (Table 3) because a large doping ratio can affect the cluster structure. It can be seen that the largest dopant ion (praseodymium) seems to have a perfect selectivity toward the central site (0% on the peripheral sites). The slope scale gradually decreases with a decrease in the ionic radius. It should be noted that we were unable to synthesize the $[Pr_9]$ compound. This could mean that the peripheral sites are too small to accommodate larger ions in such nonanuclear clusters. From Table 3, a small difference in the concentration on the two peripheral sites

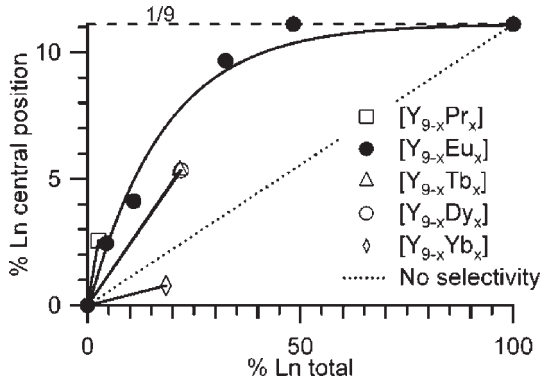

Figure 2. Doping selectivity for the different $[Y_{9-x}Ln_x]$ series. Solid lines represent the general trend of the central site doping selectivity.

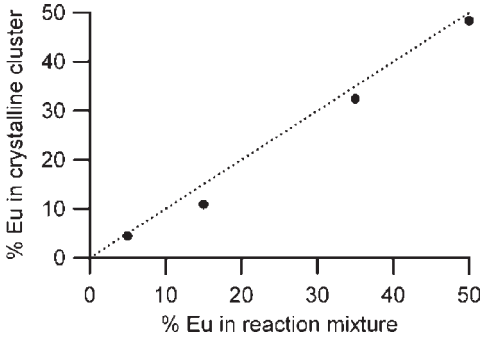

Figure 3. Correlation between the Eu^{III} concentration in the reaction and in doped Y:Eu clusters [Eu (%) = 100Eu/(Y + Eu)].

(Ln2 and Ln3) may be seen, and while small, this may be related to the μ_4-(O,OH) disorder. Indeed, on one peripheral site, Ln ions are bonded to a hydroxo group and on the second site to an oxo group, which should result in a small difference in the site size and following in the doping concentration.

These results on doped $[Y_{9-x}Ln_x]$ clusters clearly show an ionic radius size influence on the doping selectivity. This drives us to complete the XRD study by performing an analysis of the concentrations by luminescence spectroscopy. Clusters doped with Eu^{III} were chosen because their ionic radius (1.066 Å) is relatively similar to that of clusters with Y (1.019 Å) and is in agreement with the above results. A doping level discrimination on metallic sites was expected for a large range of concentrations. Eu^{III} was also retained because of its well-known characteristic visible emission.[20] In our previous experiments on pure $[Eu_9]$ compounds, resolved luminescence spectra were obtained and we were able to identify emission peaks corresponding to the different lanthanide sites (Ln1, Ln2, and Ln3).[4]

Interestingly, as shown in Figure 3, for the $[Y_{9-x}Eu_x]$ series, there is a near-perfect match between the amount of Eu^{III} input in the reaction mixture (n_r) and the total amount (n_t) found in the cluster from single-crystal XRD structure refinement.

Independent of the concentration, the central position is preferentially doped and is fully occupied at a total cluster concentration of ~50% (Table 3). Moreover, the study of the ratio (n_c/n_p) considering (Table 3) the Eu^{III}

(20) de Sa, G. F.; Malta, O. L.; Donega, C. D.; Simas, A. M.; Longo, R. L.; Santa-Cruz, P. A.; De Silva, E. F. *Coord. Chem. Rev.* **2000**, *196*, 165–195.

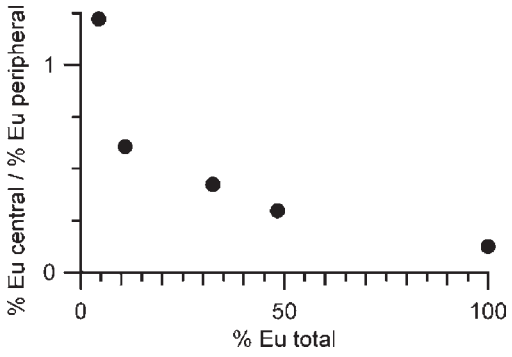

Figure 4. Variation of the ratio between the europium local population on the central and peripheral sites.

overall population (n_c) on the central site (Ln1) and those (n_p) on peripheral sites (Ln2 and Ln3) shows (Figure 4) that a low total concentration results in a relatively high population of the central sites. This behavior can be clearly seen by comparing $[Y_{4.65}Eu_{4.35}]$ and $[Y_{8.60}Eu_{0.40}]$. The first one with a high total amount of europium (48.3%) has a small n_c/n_p ratio close to 0.3 (n_c = 11.1%; n_p = 37.2%). In contrast, $[Y_{8.60}Eu_{0.40}]$ with a low total amount (4.4%) exhibits a high central/peripheral population ratio (n_c/n_p) approximating 1.2 (n_c = 2.4%; n_p = 2%; see Table 3).

Electronic Spectroscopy. In order to assess the doping specificity found by X-ray crystallography, luminescence spectroscopy of the pure $[Eu_9]$ and the doped $[Y_{9-x}Eu_x]$ compounds was studied. Europium metal centers have clear and highly resolved luminescence bands in the visible region coming from a transition from the $^5D_0$ excited state to the ^7F_n (n = 0−6) lower energy states (with $^7F_0$ being the ground state). As shown in Figure 5, the general shape and energy of the emission spectra are unchanged between the pure europium nonanuclear cluster and the corresponding doped compounds. The nonanuclear cluster contains three different lanthanide sites. The central position adopts a near-perfect square antiprism and, therefore, is highly symmetric (D_{4d}). The other eight ions are located on two slightly different bicapped trigonal prisms with very low local symmetry (C_1). Because of the sheer number of peripheral sites and the low local symmetry, a great proportion of the total luminescence intensity should arise from luminescence of Eu ions on these low-symmetry sites.

A closer look at specific bands allows for a more precise assessment of different sites. For a large majority of peaks, the general luminescence intensity ratios are not changing between pure and doped compounds but, as shown in Figure 6, some peaks are clearly gaining relative intensity when the Eu:Y decreases. The low number of peaks (only three were found) indicates that these emissions come from a highly symmetric site. It was shown by crystallography that the relative concentration of europium in central versu peripheral sites increases in lower concentration europium-doped compounds. We propose that the peaks gaining intensity arise from emission of Eu ions in the central sites.

A correlation between the intensity ratios of the luminescence peaks and the population ratios determined from X-ray crystallography is shown in Figure 7. It can be seen that for higher concentration compounds (population ratios between 0.125 and 0.5) the correlation

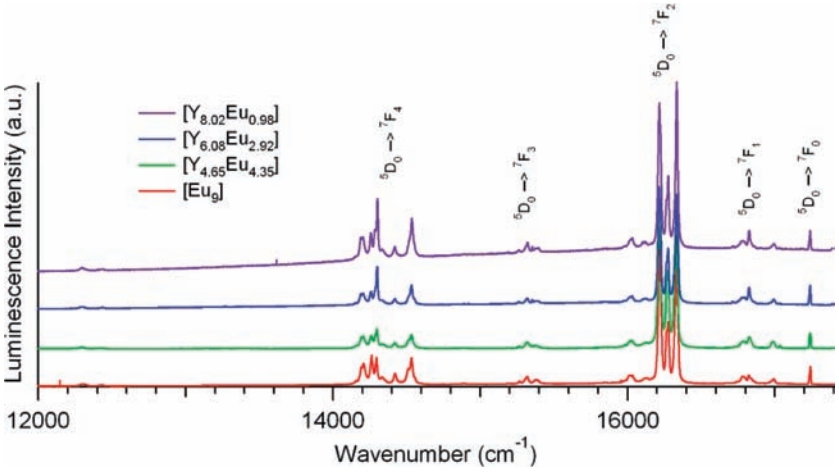

Figure 5. Luminescence spectra (83 K, λ_{ex} = 488 nm) of the pure [Eu_9] compound and of several [$Y_{9-x}Eu_x$]-doped compounds. Electronic transition bands are marked with their corresponding assignment.

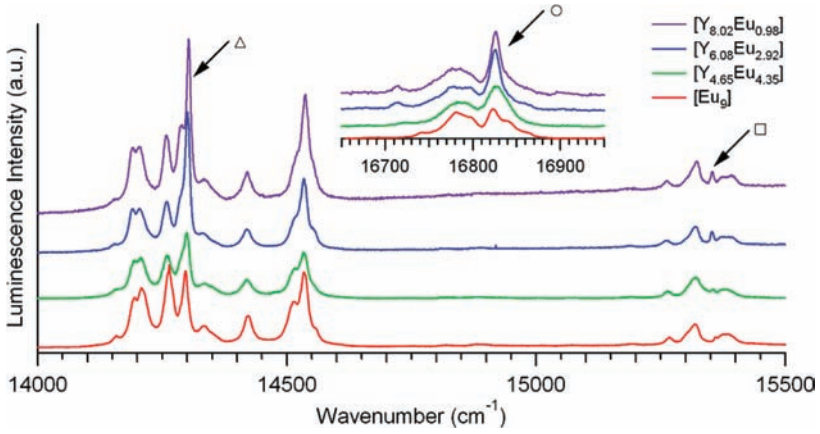

Figure 6. Close-up of the $^5D_0 \rightarrow {}^7F_{4,3,1}$ luminescence bands for the pure and doped europium compounds. Peaks with significant intensity variation are marked by arrows.

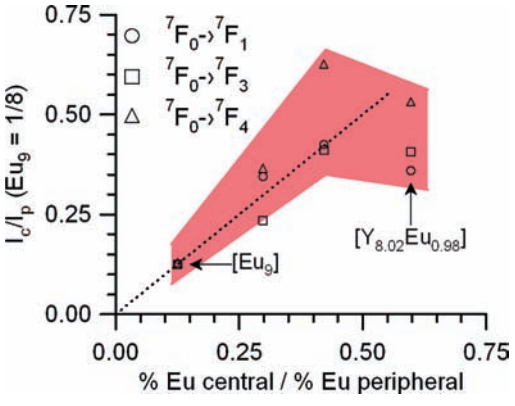

Figure 7. Comparison between the relative luminescence peak intensity ($I_{central}/I_{peripheral}$) and the population ratios found by XRD. A perfect linear relationship should follow the dashed line. Squares, triangles and circles are assigned to luminescence bands in Figure 6.

between luminescence peak intensity ratios and site populations is close to a linear relationship, indicating that site population ratios can be determined from luminescence spectra. We conclude that doping effects on the structural and electronic properties are small and that doped and pure compounds behave in a fashion similar to that of photoexcitation by a 488 nm laser. For clusters with low europium concentration and central/peripheral occupation ratios higher than 0.5, the linear relationship no longer applies and observed ratios of emission peaks are lower than expected. This specific cluster sample, [$Y_{7.9}Eu_{1.1}$], contains a mixture of [Y_9], [Y_8Eu_1], and [Y_7Eu_2] (and smaller amounts of clusters with higher doping ratios). Two kinds of [Y_8Eu_1] clusters exist where the Eu ion is either on the central site or on the peripheral site. The central site local symmetry is high (D_{4d}). In this point group, three luminescence transitions are expected to have nonzero intensity,[21] the same number as that identified by arrows in Figure 6. In contrast, the peripheral sites with C_1 local symmetry lead to multiple electric and magnetic dipole-allowed transitions, as illustrated in Figures 5 and 6. In view of these symmetry conditions, the lower excitation oscillator strengths of the [Y_8Eu_1]$_{central}$ cluster compared to the [Y_8Eu_1]$_{peripheral}$ cluster lead to the lower intensity ratios shown in Figure 7. In addition, for clusters with a higher doping ratio, excitation of the peripheral sites may lead to emission of the central sites by energy-transfer processes. Such energy-transfer processes can lead to higher luminescence intensities from the inefficiently excited central site. Figure 7, therefore, illustrates that

(21) Blasse, G. *Inorg. Chim. Acta* **1988**, *142*, 153–154.

the intensities of the luminescence peaks can be used to characterize qualitative site occupations but that care must be taken at the concentration extremes.

Conclusion

Detailed crystallographic structure determinations and luminescence spectra of doped nonanuclear clusters containing Y^{III} and Eu^{III} ions show that a chemical preference for specific sites can be used for selective doping. Luminescence spectra provide an efficient measurement of trends in selectivity.

Acknowledgment. This work has been supported by a research Ph.D. grant from the Région Rhône Alpes (to S.P.). Financial support from the Commission permanente de Coopération Franco-Québécoise (CPCFQ 61.112) and from the Natural Sciences and Engineering Research Council (Canada) is gratefully acknowledged. Single-crystal XRD studies were performed at the Centre de Diffractometrie Henri Longchambon at Université Claude Bernard Lyon 1.

Supporting Information Available: X-ray crystallographic file for compounds **1**−**8** in CIF format, a table of lanthanide concentrations determined by XRD and EDX, and a figure of Raman spectra of the doped clusters. This material is available free of charge via the Internet at http://pubs.acs.org.